Aerosol and Air Quality Research, 19: 390–398, 2019

ISSN: 1680-8584 print / 2071-1409 online
doi: 10.4209/aaqr.2018.09.0328

Evaluation of RSM for Simulating Dispersion of CO_2 Cloud in Flat and Urban Terrains

Chaojie Li, Liyan Liu*, Wei Tan**

School of Chemical Engineering and Technology, Tianjin University, Tianjin 300350, China

ABSTRACT

Accurate and reliable computational fluid dynamics (CFD) simulation of pollutant dispersion is essential for protecting human health, and the choice of turbulence model is an important parameter determining the accuracy of simulation results. This paper evaluates the ability of Reyonds stress model (RSM) to predict dispersion of carbon dioxide (CO_2) cloud, which is a typical type of heavy gas and similar to some particulate pollutants, in flat and urban terrains. The RSM simulation is conducted with stress-ω model, whereas SST k-ω two-equation model is selected as the benchmark. The simulation results are compared with the available wind tunnel measurements, and statistical performance indicators are used to obtain a comprehensive and quantitative evaluation of the performances of the two turbulence models. The results reveal that stress-ω model exhibits different capacities in flat terrain and urban terrain. Specifically, stress-ω model can present better results than SST k-ω model in flat terrain, and it performs better in the far-field region than in the near-field region. Although SST k-ω model can describe CO_2 dispersion more accurately in urban terrain, the concentration distribution reproduced by stress-ω model is still within acceptable range.

Keywords: Flat terrain; Urban terrain; Stress-ω; SST k-ω.

INTRODUCTION

Dispersion of pollutant represents a major threat to human health, and the precise prediction of pollutant concentration distribution is a prerequisite for avoiding adverse air quality impacts (Zhang *et al.*, 2011; Dodla *et al.*, 2017; Guttikunda and Jawahar, 2018). Compared with the simple Gaussian and other analytical dispersion models, computational fluid dynamics (CFD) models can provide results of the flow feature in complicated terrain simultaneously and have been widely employed to investigate pollutant dispersion (Gupta and Chan, 2016; Lateb *et al.*, 2016). Lin *et al.* (2016) studied the effects of street layout and wall heating on pollutant dispersion by CFD simulation. Huang *et al.* (2017) applied a CFD model to evaluate the impacts of the upstream building height and stack location on the dispersion of pollutant.

However, CFD models need to be established and evaluated correctly to accurately simulate pollutant dispersion. The selection of turbulence model is one of the prerequisites for CFD simulation, as it greatly affects the reproduction of flow field and the prediction of pollutant dispersion. Among the various turbulence models, the two-equation models are the main approach for turbulence modeling of the practical pollutant dispersion. However, these models are based on the isotropic Boussinesq hypothesis (Lane, 2017), which can make these models lack of the ability to predict accurately the complex flow structure along the ground, thus causing the results to be unreliable (Franke *et al.*, 2005; Longo *et al.*, 2017). To avoid the assumption of isotropy, the Reynolds stress model (RSM) can be used, which in theory should perform better than two-equation models. Yet, in some cases, the converged solution is far beyond satisfaction, and the approach cannot yield any notable gains in accuracy (Wang and McNamara, 2006; Tominaga and Stathopoulos, 2013; Peren *et al.*, 2015). For instance, Sklavounos and Rigas (2004) evaluated four turbulence models (i.e., standard k-ε model, standard k-ω model, SST k-ω model, and Speziale-Sarkar-Gatski (SSG) RSM) against Thorney Island field trials data, and found that SSG model prolonged calculation time with only constrained gains in accuracy. Bartzanas *et al.* (2007) tested four turbulence models (i.e., standard k-ε model, RNG k-ε model, realizable k-ε model, RSM) for the ventilated airflow, and found that RSM needed long convergence time and showed better performance only under low air velocities.

* Corresponding author.
Tel.: +86 2227408728; Fax: +86 2227408728
E-mail address: liuliyan@tju.edu.cn
** Corresponding author.
Tel.: +86 2227408728; Fax: +86 2227408728
E-mail address: wtan@tju.edu.cn

However, careful inspection of the relevant studies, makes clear that solid conclusion cannot be drawn by simply evaluating the results of the limited number of cases. Therefore, additional research efforts are necessary to further evaluate the performance of RSM in certain cases. In light of this, the present research aims to test the ability of RSM to predict pollutant dispersion in two types of terrains. The first type is the flat terrain, where a relatively simple flow field is observed, while the second is the urban terrain, where the complicated flow structure is produced mainly due to geometric effects (Carpentieri *et al.*, 2015).

SST *k-ω* model is characterized by an advanced near-wall treatment, taking advantages of both the *k-ε* and *k-ω* models. It gets rid of the drawback of the standard *k-ε* model that unable to describe the near-wall zone, the drawback of the modified *k-ε* models that cannot capture information in the wake volume, and the drawback of the *k-ω* model that be sensitive to free stream (Li *et al.*, 2006; Lateb *et al.*, 2013; Yu and The, 2016). Thus, SST *k-ω* model is used as the reference point for the comparison of the results. Stress-*ω* model, one of the RSM type, uses the similar boundary condition for *ω* (Sharif and Guo, 2007). Thus, both models employ the same mesh densities and near-wall grid sizes, and the results are simply determined by the turbulence models themselves. Numerical simulation of CO_2 cloud dispersion in flat and urban terrains were carried out by means of SST *k-ω* model and stress-*ω* model, and the results were tested against the available experimental data obtained from the literatures (Xing *et al.*, 2013; Tan *et al.*, 2018). Also, CO_2 cloud is a typical type of heavy gas, and therefore the results can be conducive to the simulation of some particulate pollutants dispersion.

TURBULENCE MODEL

SST k-ω Model

SST *k-ω* turbulence model is a two-equation eddy-viscosity model based on Boussinesq eddy viscosity assumption, taking both the advantage of *k-ω* model that performs better in the near-wall region and the advantage of standard *k-ε* model that is accurate and reliable for the flow outside the boundary layer, with a limiter evaluating the proper transport behavior of turbulent shear stress and a blending function transiting between *k-ω* model and *k-ε* model on the basis of the distance to the surface and on the flow variables. It has been proved to be able to predict flow field and pollutant dispersion in the atmosphere nicely (Eca and Hoekstra, 2011; Yu and The, 2016). SST is a good benchmark for higher fidelity models such as RSM, to determine if they can accurately predict the flow field distribution and pollutant dispersion (O'Brien *et al.*, 2018). Equations of the model are presented in the following:

k-equation

$$\frac{\partial k}{\partial t}+U_j\frac{\partial k}{\partial x_j}=P_k-\beta^* k\omega+\frac{\partial}{\partial x_j}\left[\left(\nu+\sigma_k\nu_t\right)\frac{\partial k}{\partial x_j}\right] \tag{1}$$

ω-equation

$$\frac{\partial \omega}{\partial t}+U_j\frac{\partial \omega}{\partial x_j}=\alpha S^2-\beta\omega^2+\frac{\partial}{\partial x_j}\left[\left(\nu+\sigma_\omega\nu_t\right)\frac{\partial \omega}{\partial x_j}\right]+2\left(1-F_1\right)\sigma_{w2}\frac{1}{\omega}\frac{\partial k}{\partial x_i}\frac{\partial \omega}{\partial x_i} \tag{2}$$

The kinematic eddy viscosity is calculated from

$$\nu_t=\frac{a_1 k}{\max(a_1\omega, SF_2)} \tag{3}$$

where *S* is the strain rate magnitude.

The closure coefficients and auxiliary relations are given by

$$F_2=\tanh\left\{\left[\max\left(\frac{2\sqrt{k}}{B^*\omega y},\frac{500\nu}{y^2\omega}\right)\right]^2\right\} \tag{4}$$

where *y* is the distance to the next surface.

$$P_k=\min\left(\tau_{ij}\frac{\partial U_i}{\partial x_j},10\beta^* k\omega\right) \tag{5}$$

$$F_1=\tanh\left\{\left\{\min\left[\max\left(\frac{2\sqrt{k}}{B^*\omega y},\frac{500\nu}{y^2\omega}\right),\frac{4\sigma_{\omega 2}k}{CD_{k\omega}y^2}\right]\right\}^4\right\} \tag{6}$$

$$CD_{k\omega}=\max\left(2\rho\sigma_{\omega 2}\frac{1}{\omega}\frac{\partial k}{\partial x_i}\frac{\partial \omega}{\partial x_i},10^{-10}\right) \tag{7}$$

The constants are summarized as $\phi = \phi_1 F_1 + \phi_2(1 - F_1)$, with $\phi = \sigma_k, \sigma_\omega, \alpha, \beta, a_1 = 0.31, \alpha_1 = 5/9, \alpha_2 = 0.44, \beta_1 = 3/40, \beta_2 = 0.0828, \beta^* = 0.09, \sigma_{k1} = 0.85, \sigma_{k2} = 1, \sigma_{\omega 1} = 0.5, \sigma_{\omega 2} = 0.856$.

Stress-ω Model

RSM (Launder *et al.*, 1975) resolves directly a transport equation for each term of the Reynolds stress tensor separately using differential equations, taking the anisotropy of turbulence into account and making up for the deficiencies of the Boussinesq approximation. According to the modeling of the pressure-strain and dissipation-rate terms, the CFD-Fluent provides numerous types of RSM. Stress-*ω* model, a stress-transport model based on the omega equation and Launder-Reece-Rodi (LRR) model (Launder *et al.*, 1975), is considered in this paper. Stress-*ω* model is similar to *k-ω* model, mainly reflected in the transport equation for *ω* and the wall boundary condition for *ω* (Sharif and Guo, 2007). The model equations are expressed as follows:

Stress-equation

$$\frac{\partial \tau_{ij}}{\partial t}+U_k\frac{\partial \tau_{ij}}{\partial x_k}=-P_{ij}+\frac{2}{3}\beta^*\omega k\delta_{ij}-\Pi_{ij}+\frac{\partial}{\partial x_k}\left[\left(\nu+\sigma^*\nu_t\right)\frac{\partial \tau_{ij}}{\partial x_k}\right] \quad (8)$$

ω-equation

$$\frac{\partial \omega}{\partial t}+U_j\frac{\partial \omega}{\partial x_j}=\alpha\frac{\omega}{k}\tau_{ij}\frac{\partial U_i}{\partial x_j}-\beta\omega^2+\frac{\partial}{\partial x_j}\left[\left(\nu+\sigma\nu_t\right)\frac{\partial \omega}{\partial x_j}\right] \quad (9)$$

The pressure-strain correlation is given as

$$\Pi_{ij}=\beta^*C_1\omega\left(\tau_{ij}+\frac{2}{3}k\delta_{ij}\right)-\hat{\alpha}\left(P_{ij}-\frac{2}{3}P\delta_{ij}\right)-\hat{\beta}\left(D_{ij}-\frac{2}{3}P\delta_{ij}\right)-\hat{\gamma}k\left(S_{ij}-\frac{1}{3}S_{kk}\delta_{ij}\right) \quad (10)$$

where

$$P_{ij}=\tau_{im}\frac{\partial U_j}{\partial x_m}+\tau_{jm}\frac{\partial U_i}{\partial x_m} \quad (11)$$

$$D_{ij}=\tau_{im}\frac{\partial U_m}{\partial x_j}+\tau_{jm}\frac{\partial U_m}{\partial x_i} \quad (12)$$

$$P=\frac{1}{2}P_{kk} \quad (13)$$

The closure coefficients are defined as C_1 = 9/5, C_2 = 13/25, α = 13/25, σ = 1/2, σ^* = 1/2, β_0 = 9/125, β^*_0 = 9/100, $\beta=\beta_0 f_\beta$, $\beta^*=\beta^*_0 f_{\beta^*}$, $\hat{\alpha}=\frac{8+C_2}{11}$, $\hat{\beta}=\frac{8C_2-2}{11}$, $\hat{\gamma}=\frac{60C_2-4}{55}$, $f_\beta=\frac{1+70\chi_\omega}{1+80\chi_\omega}$, $\chi_\omega=\left|\frac{\Omega_{ij}\Omega_{jk}S_{ki}}{\left(\beta^*_0\omega\right)^3}\right|$, $S_{ij}=\frac{1}{2}\left(\frac{\partial U_i}{\partial x_j}+\frac{\partial U_j}{\partial x_x}\right)$, $\Omega_{ij}=\frac{1}{2}\left(\frac{\partial U_i}{\partial x_j}-\frac{\partial U_j}{\partial x_x}\right)$, $\chi_k=\frac{1}{\omega^3}\frac{\partial k}{\partial x_j}\frac{\partial \omega}{\partial x_j}$, $f_{\beta^*}=\begin{cases}1 & \chi_k\le 0\\ \frac{1+640\chi_k^2}{1+400\chi_k^2} & \chi_k>0\end{cases}$.

STATISTICAL MODEL PERFORMANCE EVALUATION METHOD

Five performance measures (Hanna *et al.*, 2004), including the fractional bias (FB), the geometric mean bias (MG), the normalized mean square error (NMSE), the geometric variance (VG), and the fraction of predictions within a factor of two of observations (FAC2), defined as below, were used to obtain a comprehensive and quantitative evaluation of the performances of these two turbulence models for dispersion of CO_2 cloud.

$$FB=\frac{\left(\overline{C}_O-\overline{C}_P\right)}{0.5\left(\overline{C}_O+\overline{C}_P\right)} \quad (14)$$

$$MG=\exp\left(\overline{\ln C_O}-\overline{\ln C_P}\right) \quad (15)$$

$$NMSE=\frac{\overline{\left(C_O-C_P\right)^2}}{\overline{C}_O\overline{C}_P} \quad (16)$$

$$VG=\exp\left[\overline{\left(\ln C_o-\ln C_p\right)^2}\right] \quad (17)$$

$$FAC2 = \text{fraction of data that satisfy } 0.5\le C_p/C_o\le 2.0 \quad (18)$$

where C_p was model predictions of concentration, C_o was observations of concentration, and $\overline{C}$ was average over the data set.

According to the literature (Hanna *et al.*, 2004), FB = 0, MG = 1.0, NMSE = 0, VG = 1.0 and FAC2 = 1.0 represent the perfect model, and –0.3 < FB < 0.3, 0.7 < MG < 1.3, NMSE < 4, VG < 1.6 and 0.5 < FAC2 represent the acceptable range.

EVALUATION OF STRESS-ω MODEL IN FLAT TERRAIN

Description of Wind Tunnel Experiment Considered

This experiment (Xing *et al.*, 2013) conducted by the Beijing Institute of Technology was simulated, and the simulation results were compared with experimental data to conduct the evaluation of stress-ω model for simulating dispersion of CO_2 cloud in flat terrain. The experiment was implemented in a 6.4-m-wide, 5.2-m-high wind tunnel located in Zhangjiakou. The sonic anemometer was placed at the wind inlet at a height of 2 m to measure the wind speed. In the trials, the CO_2 inlet had a radius of 0.01 m and CO_2 of 99.9% by volume was oriented vertically upwards under atmospheric pressure, which could realize the simulation of pollutant dispersion from a point release at the ground level (Shen *et al.*, 2017; Wingstedt *et al.*, 2017). Four different cases with CO_2 flow rates of 166.7 L min^{-1}, 200 L min^{-1}, 250 L min^{-1}, 300 L min^{-1}, corresponding to the flow speeds of 8.8 m s^{-1}, 10.6 m s^{-1}, 13.3 m s^{-1} and 15.9 m s^{-1}, were carried out. Ten sensors were arrayed in the central line through the jet nozzle along the downwind direction, with the distances of 0.5 m, 1 m, 1.5 m, 2 m, 2.5 m, 3 m, 4 m, 6 m, 8 m, 10 m, to acquire CO_2 concentration data.

Fluent CFD Model Set-up

The rectangular domain with a cross-section of 6.4 m ×

5.2 m was developed in this work, as shown in Fig. 1. The front of the domain was air inlet, and the rear, named outlet, remained open to the atmosphere. The wind direction was parallel to the bottom from the front to the rear, and a fully developed flow can be established in the computational domain. Structural grid was adopted to discrete the computational domain. Three quantities of cells (i.e., 1133136, 1890864, and 3828672) were utilized to perform the grid sensitivity analysis. SST *k*-*ω* model was chosen here. CO_2 concentration in the central ground at 200 s after release with the flow speed of 8.8 m s^{-1} was compared, as shown in Fig. 2. It was found that the change in the results was limited and the grid with 1890864 cells was chosen. The minimum horizontal grid size was about 0.0025 m at CO_2 inlet. The minimum grid size in the vertical direction was 0.02 m near the ground and expanding away from it with an expansion factor of 1.1 to 0.08 m.

Difference between the wind condition in the experiment and in the simulation can also lead to the deviation between the experimental and simulated cloud concentration (Garcia-Sanchez *et al.*, 2014; Weerasuriya *et al.*, 2018; Zhang *et al.*, 2018). The inlet boundary condition in the CFD simulation was obtained considering the local atmospheric stability class of "*F*" at the field site. The wind velocity profile was defined by the power law (Tominaga *et al.*, 2008; Wu *et al.*, 2014) to describe the boundary layer.

$$U_Z = U_0 \times \left(\frac{Z}{Z_0}\right)^{\alpha} \tag{19}$$

where, the reference velocity U_0 and the reference height Z_0 were respectively 0.37 m s^{-1} and 2 m, and the value of the power-law exponent α was set as 0.3 according to the literature (Xing *et al.*, 2013). The power law profile was included into the FLUENT code through user-defined functions (UDFs). Air temperature and CO_2 temperature were obtained based on experimental data. The initial and boundary conditions are summarized in Table 1.

Comparison of CO_2 Concentration with Various Turbulence Models

The two cases with CO_2 flow speeds of 8.8 m s^{-1} (166.7 L min^{-1}) and 13.3 m s^{-1} (250 L min^{-1}) were modeled, respectively. The simulation strategy involved a steady-state simulation for flow field and a transient simulation for CO_2 cloud dispersion, with the time step of 0.05 s. CO_2 concentration data in the central ground line parallel to the wind velocity at 200 s, when the flow field has been relatively steady, were measured. Figs. 3 and 4 show the comparisons between the experimental data and the simulation results using various turbulence models.

The comparisons between experimental data and simulation results show that both of the two turbulence models had a weak accuracy in the near-field region, where the source flow showed strong interaction with wind flow. With the vertical momentum of the source, vortices can be formed in both the upstream and downstream of CO_2 inlet, and the flow in the near-field region was dominated by the vortices (Wingstedt *et al.*, 2017). This created highly anisotropic turbulent structure. For the case with CO_2 flow speed of 8.8 m s^{-1}, stress-*ω* model provided the better results in both near- and far-field regions in comparison to SST *k*-*ω* model, although SST *k*-*ω* model captured the maximum value and the position corresponding to the maximum value. Especially in the near-field region, SST *k*-*ω* model significantly underestimated CO_2 concentration and the advantage of stress-*ω* model was more pronounced. For the case with CO_2 flow speed of 13.3 m s^{-1}, the simulation results from stress-*ω* model were in good agreement with the experimental data with respect to both the magnitude and trend. It successfully captured the position corresponding to the maximum value and the variation of CO_2 concentration in the near-field region that

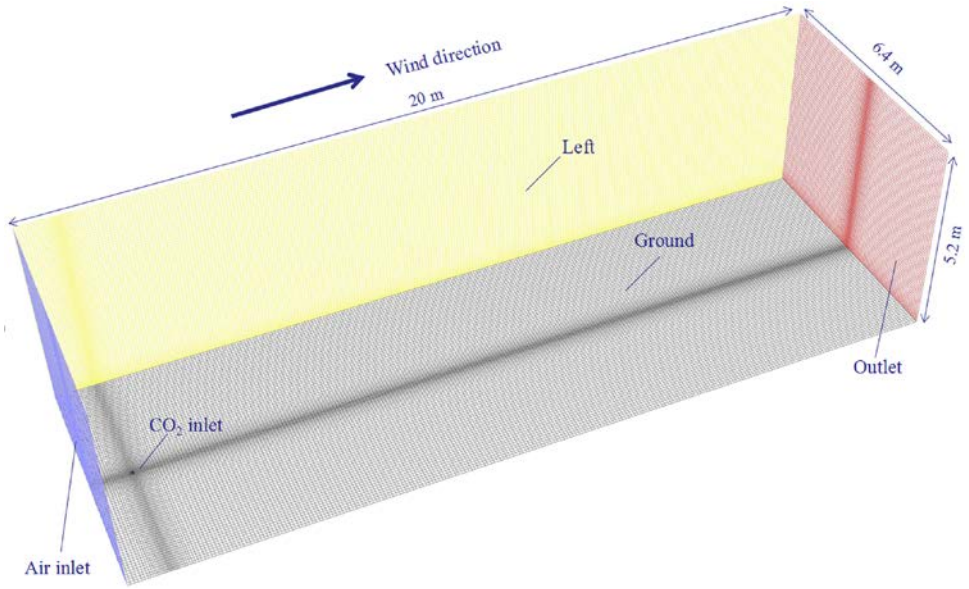

Fig. 1. Computational grid for flat terrain.

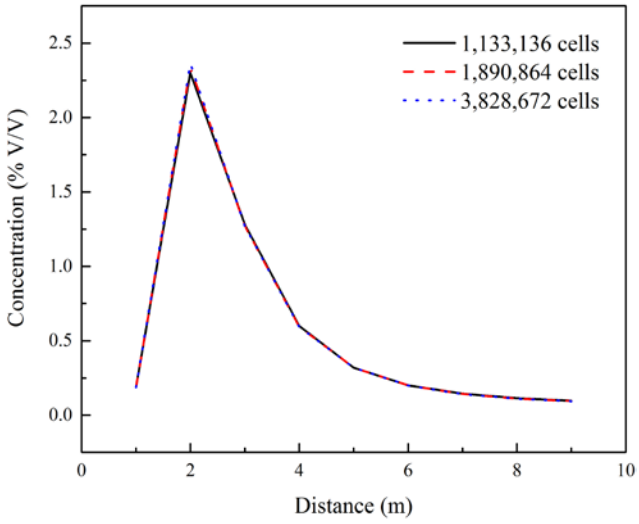

Fig. 2. Grid independence analysis for flat terrain.

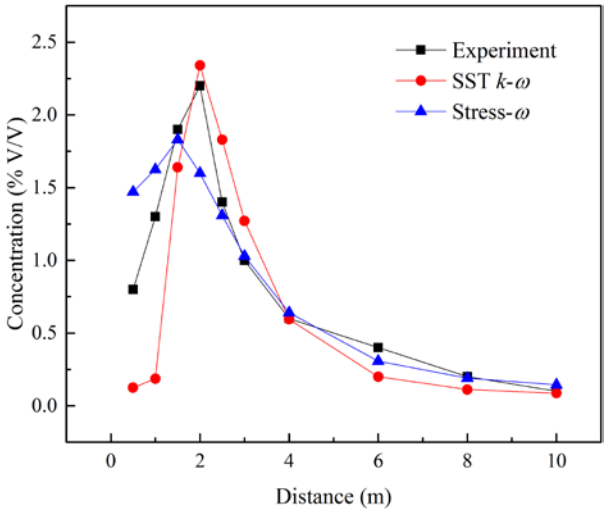

Fig. 3. CO_2 concentration in the central ground line parallel to wind flow with CO_2 flow speed of 8.8 m s^{-1}.

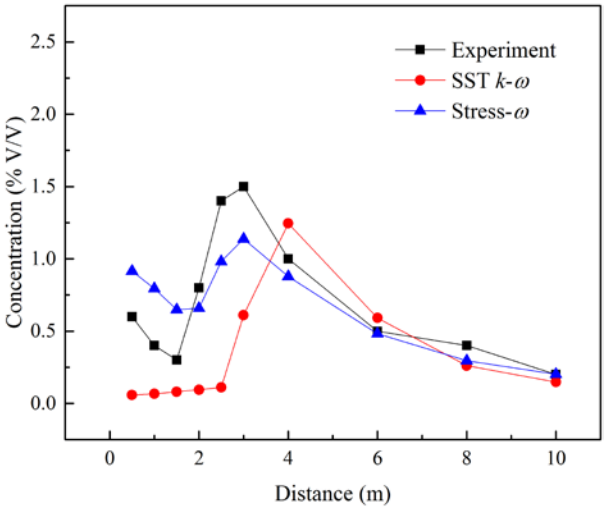

Fig. 4. CO_2 concentration in the central ground line parallel to wind flow with CO_2 flow speed of 13.3 m s^{-1}.

Table 1. The boundary conditions used in the simulation for flat terrain.

Parameters	Setup
Air inlet	Velocity-inlet
CO_2 inlet	Velocity-inlet
Ground	Wall, roughness = 5×10^{-3} m
Top, left, right	Symmetry
Outlet	Outflow
Air temperature	293 K
CO_2 temperature	277 K

decreased firstly then increased with distance. Whereas, the results predicted by SST *k-ω* model exhibited different law that CO_2 concentration increased with distance. Also, the position of maximum point appeared a certain degree of deviation.

As shown in Table 2, all five performance measures for stress-*ω* model were within acceptable range. While, some measures for SST *k-ω* model were outside, as highlighted in gray. And the main reason is that the strong interaction between wind flow and source flow creates highly anisotropic turbulent structure in the near-field region, and SST *k-ω* model lacks the capacity to predict accurately the complex flow structure, causing the larger deviation between simulation result and experimental data. The results of the validation metrics support that stress-*ω* model can produce much better results compared with SST *k-ω* model in flat terrain. Therefore, the enhancement of accuracy of simulation results can be considered to be worth the increased computational time.

EVALUATION OF STRESS-*ω* MODEL IN URBAN TERRAIN

Description of Wind Tunnel Experiment Considered

In this work, urban terrain was referred to as the street canyon, which was the basic element of urban fabric. In the street canyon, cloud concentration field was mainly governed by the wind field induced by the geometric effects, consisting of wakes, stagnating zones, recirculation, and preferential paths (Park *et al.*, 2015; Mei *et al.*, 2016; Tominaga and Stathopoulos, 2016; Nosek *et al.*, 2017). The experiment (Tan *et al.*, 2018) focused on CO_2 cloud dispersion in the street canyon was simulated for the evaluation of stress-*ω* model in cloud dispersion in urban terrain. This experiment was carried out in a 0.75-m-wide, 0.5-m-high wind tunnel. Spires and roughness elements were installed in front of the building arrays to develop the boundary layer. The wind direction was perpendicular to the target street canyon. The incident velocity was measured in the wind tunnel with anemometer at the middle line upstream of the test section to calculate mean velocity and turbulence intensity profile. The reference mean velocity at the building height was 0.66 m s^{-1} and the exponent α in the power law profile was 0.308. The street canyons were modeled using box-shaped blocks and the CO_2 inlet was a

Table 2. Summary of the statistical performance for flat terrain.

Flow rate (m s^{-1})	Model	FB	MG	NMSE	VG	FAC2
Perfect model		0	1.0	0	1.0	1.0
Acceptable range		–0.3 to 0.3	0.7–1.3	< 4.0	< 1.6	> 0.5
8.8	SST *k-ω*	0.166	1.618	0.252	2.282	0.8
	Stress-*ω*	–0.024	0.946	0.0939	1.077	1.0
13.3	SST *k-ω*	0.739	3.107	1.505	9.475	0.4
	Stress-*ω*	0.015	0.942	0.147	1.173	0.9

circle with a radius of 0.0065 m located in the target canyon. CO_2 of 99.9% by volume was jetted vertically upwards at ground level with the flow rate of 4.48 L min^{-1} under atmospheric pressure, corresponding to the flow speed of 0.5628 m s^{-1}. These two box-shaped blocks used in the experiment had dimensions of 0.2 × 0.05 × 0.05 m^3 (L × W × H) and 0.05 × 0.05 × 0.05 m^3 (L × W × H) respectively, forming five streets connected through a streamwise street. Four sensors based on Infra-Red and detector technology were respectively located near the CO_2 inlet, on the leeward side, on the windward side and above the windward building to acquire CO_2 concentration data. Considering CO_2 inlet as the origin with *y* measured as positive in the downwind direction and *z* positive upwards, the four measuring points' coordinates were respectively Point 1 (0, –0.025, 0.025), Point 2 (0.125, –0.025, 0.025), Point 3 (0.125, 0.025, 0.025), and Point 4 (0, 0.05, 0.05).

Fluent CFD Model Set-up

The size of the domain was determined following the wind-tunnel geometry, with width 0.75 m, and height 0.5 m, as shown in Fig. 5. A fully structured grid was built. SST *k-ω* model was also chosen to perform grid-sensitivity analysis among three types of grids, with the number of 1380774, 3183462 and 6135432. Fig. 6 shows the influence of grid size on CO_2 concentration in the centerline of the street at z = 0.025 m and at 15 s after release. The grid with 3,183,462 cells was selected keeping in view both the computing time and the solution accuracy. The grid size in the canyon was 0.005 m and expanding away from it to 0.01 m. Further refinement close to walls and ground was performed.

The inlet boundary conditions used in the simulation were based on the measured incident vertical profiles of mean wind velocity and turbulence intensity in the wind tunnel experiment. The vertical profiles of mean wind velocity, turbulent kinetic energy and its specific dissipation rate were used to describe the variation of wind as a function of height.

$$\frac{\bar{v}(z)}{\bar{v}(z_H)} = \left(\frac{z}{z_H}\right)^{0.308} \tag{20}$$

where $\bar{v}(z)$ was the mean velocity at z.

$$k(z) = 1.5 \cdot \bar{v}^2(z_H) \cdot I^2(z_H) \cdot \left(\frac{z_H}{z}\right)^{0.566} \tag{21}$$

where *I* was the turbulence intensity.

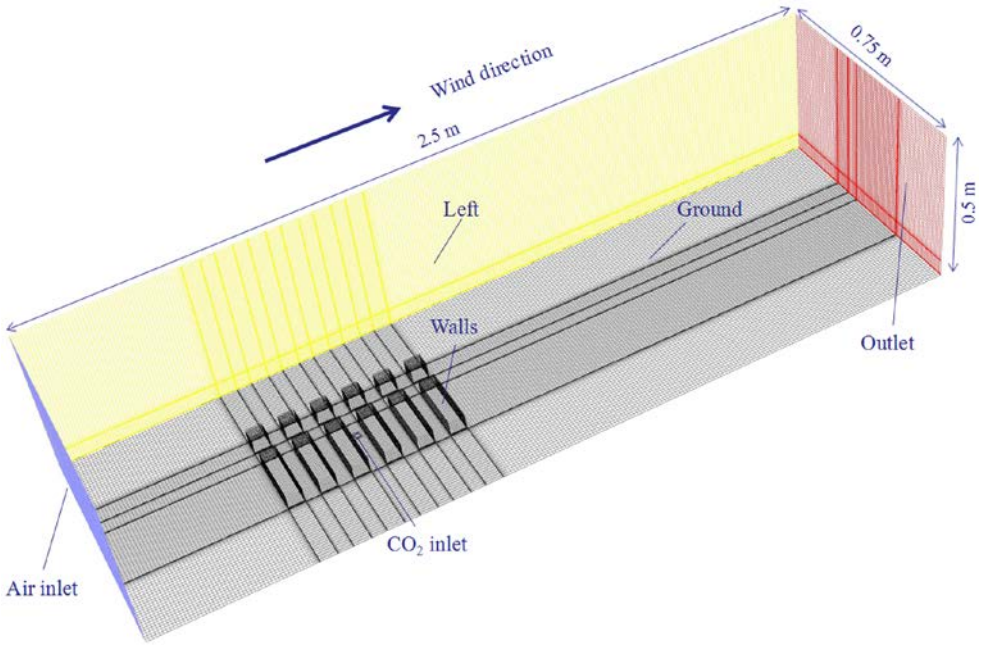

Fig. 5. Computational grid for urban terrain.

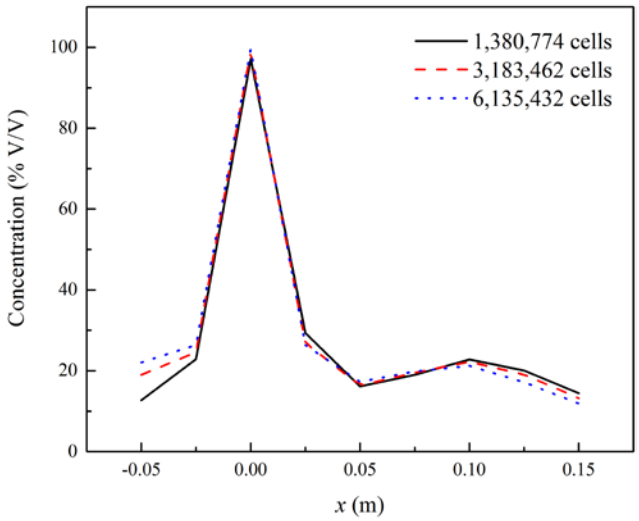

Fig. 6. Grid independence analysis for urban terrain.

$$\omega(z)=\frac{2.236\cdot\overline{v}(z_H)\cdot I(z_H)\cdot\left(\frac{z_H}{z}\right)^{0.595}}{L_H} \quad (22)$$

where L was turbulence integral scale.

According to the experiment, CO_2 was released at an average speed of 0.5628 m s^{-1}. The initial and boundary conditions used in the simulation are shown in Table 3.

Comparison of CO_2 Concentration with Various Turbulence Models

The time step was 1×10^{-3} s in the transient simulation to assure Courant number was less than 1. The calculation was carried out up to t =15 s, by which time CO_2 concentration had reached a relative stable value. CO_2 concentration data at the measuring points were calculated. As shown in Fig. 7, CO_2 concentration in urban terrain was larger than in flat terrain due to the blocking effect of spreading downstream. Simulation results reproduced by stress-ω model agreed worse with experimental data at all the four measuring points. It underestimated CO_2 concentration near the CO_2 inlet and on the windward side, and overestimated the concentration on the leeward side and above the windward building. However, SST k-ω model underestimated the concentration above the windward building, overestimated the concentration on both the leeward side and windward building, and had the closest coincidence with experimental data near the CO_2 inlet.

As shown in Table 4, the simulation results from the two turbulence models were all within acceptable range. And the results also reveal that the performance of stress-ω model was worse than that of SST k-ω model. This may be due to two reasons. The first is that stress-ω model requires more empirical data which can vary from one flow to another, and the advantage itself for complex turbulent flow in urban terrain may be not significant. The second is that an advanced near-wall treatment may play a more important role than the consideration of turbulence anisotropy. In other words, the advantage of SST k-ω that automatically switches between the low- and high-Re number ω formulation is more significant for the prediction accuracy of flow structure in urban terrain. Coupled with the extra computational effort for the higher number of differential equations, stress-ω model still needs further investigation and optimization for accounting for various effects of complex turbulent flow in urban terrain.

Table 3. The boundary conditions used in the simulation for urban terrain.

Parameters	Setup
Air inlet	Velocity-inlet
CO_2 inlet	Velocity-inlet
Ground, walls	Wall, roughness = 10^{-5} m
Top, left, right	Symmetry
Outlet	Outflow
Air temperature	290.8 K
CO_2 temperature	290.8 K

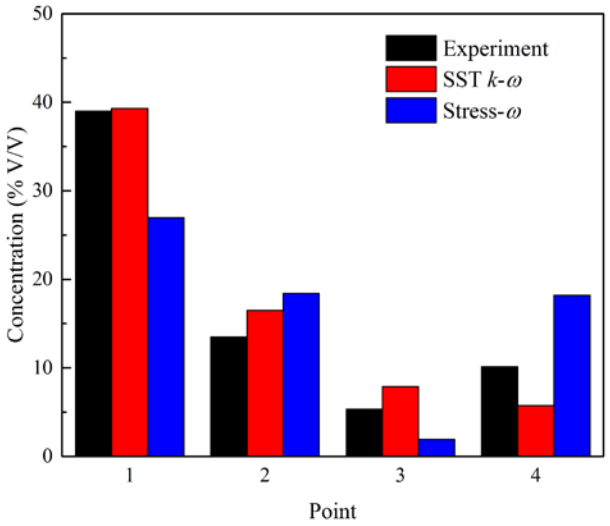

Fig. 7. CO_2 concentration at the measuring points.

CONCLUSIONS

This paper performs a comparison of CO_2 concentration data obtained by SST k-ω model (as the benchmark) and stress-ω model with the available wind tunnel test data, to evaluate the applicability and accuracy of RSM for simulating cloud dispersion in flat terrain and urban terrain. The results reflect that stress-ω model shows better agreement with experimental data compared to SST k-ω model in flat terrain. And it performs better in the far field than in the near-field region. The performance measures for stress-ω model are all within acceptable range, while some measures for SST k-ω model are outside. For urban terrain, the performance of stress-ω turbulence model is worse than that of SST k-ω model, although the simulation results are still within acceptable range. This leads to the conclusion that the capacity of RSM is concerned with its application scenario. Specially, stress-ω model exhibits

Table 4. Summary of the statistical performance for urban terrain.

Model	FB	MG	NMSE	VG	FAC2
Perfect model	0	1.0	0	1.0	1.0
Acceptable range	–0.3 to 0.3	0.7–1.3	< 4.0	< 1.6	> 0.5
SST *k-ω*	–0.021	0.993	0.0297	1.138	1.0
Stress-*ω*	0.037	1.133	0.221	1.504	0.75

better performance for simulation of the relatively simple flow field in flat terrain and SST *k-ω* model is still ascendant for the complicated flow structure in urban terrain. The conclusions are of primary importance when deciding which turbulence model to use and drafting guidelines on the use of CFD for the simulation of pollutant dispersion in flat and urban terrains.

It is recommended that the comparison of two-equation model and RSM be made in different terrain conditions. Also, additional experimental data examining the flow structure are necessary to provide a quantitative explanation for the limitation of turbulence models.

ACKNOWLEDGMENTS

This work was supported by The National Key Research and Development Program of China (grant number 2016YFC0801900); Tianjin Science and Technology Planning Project (grant number 15ZCZDSF00550).

NOMENCLATURE

k	Turbulent kinetic energy
t	Time
ε	Turbulent dissipation rate
ω	Specific turbulent dissipation rate
δ_{ij}	Kronecker delta function
δ	Boundary layer thickness
v	Turbulence dynamic viscosity
v_t	Turbulence kinematic viscosity
ρ	Density
τ_{ij}	Reynolds stress tensor
S	The strain rate magnitude
P_k	The production limiter to prevent turbulence buildup in stagnation regions
U	Velocity vector
i, j	Grid node in x and y direction
Ω_{ij}	The mean-strain-rate tensor
S_{ki}	The mean-rotation-tensor

REFERENCES

Bartzanas, T., Kittas, C., Sapounas, A.A. and Nikita-Martzopoulou, C. (2007). Analysis of airflow through experimental rural buildings: Sensitivity to turbulence models. *Biosyst. Eng.* 97: 229–239.

Carpentieri, M. and Robins, A.G. (2015). Influence of urban morphology on air flow over building arrays. *J. Wind Eng. Ind. Aerodyn.* 145: 61–74.

Dodla, V.B.R., Gubbala, C.S. and Desamsetti, S. (2017). Atmospheric dispersion of $PM_{2.5}$ precursor gases from two major thermal power plants in Andhra Pradesh, India. *Aerosol Air Qual. Res.* 17: 381–393.

Eca, L. and Hoekstra, M. (2011). Numerical aspects of including wall roughness effects in the SST *k-ω* eddy-viscosity turbulence model. *Comput. Fluids* 40: 299–314.

Franke, M., Wallin, S. and Thiele, F. (2005). Assessment of explicit algebraic Reynolds-stress turbulence models in aerodynamic computations. *Aerosp. Sci. Technol.* 9: 573–581.

Garcia-Sanchez, C., Philips, D.A. and Gorle, C. (2014). Quantifying inflow uncertainties for CFD simulations of the flow in downtown Oklahoma City. *Build. Environ.* 78: 118–129.

Gupta, S. and Chan, S. (2016). A CFD based explosion risk analysis methodology using time varying release rates in dispersion simulations. *J. Loss Prev. Process Ind.* 39: 59–67.

Guttikunda, S.K. and Jawahar, P. (2018). Evaluation of particulate pollution and health impacts from planned expansion of coal-fired thermal power plants in India using WRF-CAMx modeling system. *Aerosol Air Qual. Res.* 18: 3187-3202.

Hanna, S.R., Hansen, O.R. and Dharmavaram, S. (2004). FLACS CFD air quality model performance evaluation with Kit Fox, MUST, Prairie Grass, and EMU observations. *Atmos. Environ.* 38: 4675–4687.

Huang, Y.D., Song, Y., Xu, X., He, W.R. and Kim, C.N. (2017). Impacts of upstream building height and stack location on pollutant dispersion from a rooftop stack. *Aerosol Air Qual. Res.* 17: 1837–1855.

Lane, G.L. (2017). Improving the accuracy of CFD predictions of turbulence in a tank stirred by a hydrofoil impeller. *Chem. Eng. Sci.* 169: 188–211.

Lateb, M., Masson, C., Stathopoulos, T. and Bedard, C. (2013). Comparison of various types of k-epsilon models for pollutant emissions around a two-building configuration. *J. Wind Eng. Ind. Aerodyn.* 115: 9–21.

Lateb, M., Meroney, R.N., Yataghene, M., Fellouah, H., Saleh, F. and Boufadel, M.C. (2016). On the use of numerical modelling for near-field pollutant dispersion in urban environments - A review. *Environ. Pollut.* 208: 271–283.

Launder, B.E., Reece, G.J. and Rodi, W. (1975). Progress in the development of a Reynolds-stress turbulence closure. *J. Fluid Mech.* 68: 537–566.

Li, X.X., Liu, C.H., Leung, D.Y.C. and Lam, K.M. (2006). Recent progress in CFD modelling of wind field and pollutant transport in street canyons. *Atmos. Environ.* 40: 5640–5658.

Lin, L., Hang, J., Wang, X.X., Wang, X.M., Fan, S.J., Fan,

Q. and Liu, Y.H. (2016). Integrated effects of street layouts and wall heating on vehicular pollutant dispersion and their reentry toward downstream canyons. *Aerosol Air Qual. Res.* 16: 3142–3163.

Longo, R., Ferrarotti, M., Sanchez, C.G., Derudi, M. and Parente, A. (2017). Advanced turbulence models and boundary conditions for flows around different configurations of ground-mounted buildings. *J. Wind Eng. Ind. Aerodyn.* 167: 160–182.

Mei, D., Deng, Q.H., Wen, M. and Fang, Z. (2016). Evaluating dust particle transport performance within urban street canyons with different building heights. *Aerosol Air Qual. Res.* 16: 1483–1496.

Nosek, S., Kukacka, L., Jurcakova, K., Kellnerova, R. and Janour, Z. (2017). Impact of roof height non-uniformity on pollutant transport between a street canyon and intersections. *Environ. Pollut.* 227: 125–138.

O'Brien, J.M., Young, T.M., Early, J.M. and Griffin, P.C. (2018). An assessment of commercial CFD turbulence models for near wake HAWT modelling. *J. Wind Eng. Ind. Aerodyn.* 176: 32–53.

Park, S.J., Kim, J.J., Kim, M.J., Park, R.J. and Cheong, H.B. (2015). Characteristics of flow and reactive pollutant dispersion in urban street canyons. *Atmos. Environ.* 108: 20–31.

Peren, J.I., van Hooff, T., Leite, B.C.C. and Blocken, B. (2015). CFD analysis of cross-ventilation of a generic isolated building with asymmetric opening positions: Impact of roof angle and opening location. *Build. Environ.* 85: 263–276.

Sharif, M.A.R. and Guo, G. (2007). Computational analysis of supersonic turbulent boundary layers over rough surfaces using the *k-ω* and the stress-*ω* models. *Appl. Math. Model.* 31: 2655–2667.

Shen, Z., Cui, G.X. and Zhang, Z.S. (2017). Turbulent dispersion of pollutants in urban-type canopies under stable stratification conditions. *Atmos. Environ.* 156: 1–14.

Sklavounos, S. and Rigas, F. (2004). Validation of turbulence models in heavy gas dispersion over obstacles. *J. Hazard. Mater.* 108: 9–20.

Tan, W., Li, C.J., Wang, K., Zhu, G.R., Wang, Y. and Liu, L.Y. (2018). Dispersion of carbon dioxide plume in street canyons. *Process Saf. Environ. Prot.* 116: 235–242.

Tominaga, Y., Mochida, A., Yoshie, R., Kataoka, H., Nozu, T., Yoshikawa, M. and Shirasawa, T. (2008). AIJ guidelines for practical applications of CFD to pedestrian wind environment around buildings. *J. Wind Eng. Ind. Aerodyn.* 96: 1749–1761.

Tominaga, Y. and Stathopoulos, T. (2013). CFD simulation of near-field pollutant dispersion in the urban environment: A review of current modeling techniques. *Atmos. Environ.* 79: 716–730.

Tominaga, Y. and Stathopoulos, T. (2016). Ten questions concerning modeling of near-field pollutant dispersion in the built environment. *Build. Environ.* 105, 390–402.

Wang, X. and McNamara, K.F. (2006). Evaluation of CFD simulation using RANS turbulence models for building effects on pollutant dispersion. *Environ. Fluid Mech.* 6: 181–202.

Weerasuriya, A.U., Hu, Z.Z., Zhang, X.L., Tse, K.T., Li, S. and Chan, P.W. (2018). New inflow boundary conditions for modeling twisted wind profiles in CFD simulation for evaluating the pedestrian-level wind field near an isolated building. *Build. Environ.* 132: 303–318.

Wingstedt, E.M.M., Osnes, A.N., Akervik, E., Eriksson, D. and Reif, B.A.P. (2017). Large-eddy simulation of dense gas dispersion over a simplified urban area. *Atmos. Environ.* 152: 605–616.

Wu, S.C., Jo, Y.M. and Park, Y.K. (2014). Effect of heat recovery from flue gas on the local humidity and NO_x dispersion in a thermal power station. *Aerosol Air Qual. Res.* 14: 840–849.

Xing, J., Liu, Z.Y., Huang, P., Feng, C.G., Zhou, Y., Zhang, D.P. and Wang, F. (2013). Experimental and numerical study of the dispersion of carbon dioxide plume. *J. Hazard. Mater.* 256: 40–48.

Yu, H.S. and The, J. (2016). Validation and optimization of SST *k-ω* turbulence model for pollutant dispersion within a building array. *Atmos. Environ.* 145: 225–238.

Zhang, Y.W., Gu, Z.L., Cheng, Y., Shen, Z.X., Dong, J.G. and Lee, S.C. (2011). Measurement study of diurnal variations of $PM_{2.5}$ mass concentrations and affecting factors on pollutant dispersion in urban street canyons under weak-wind conditions in Xi'an. *Aerosol Air Qual. Res.* 12: 1261–1268.

Zhang, Y.W., Gu, Z.L. and Yu, C.W. (2017). Review on numerical simulation of airflow and pollutant dispersion in urban street canyons under natural background wind condition. *Aerosol Air Qual. Res.* 18: 780–789.

Received for review, September 2, 2018
Revised, December 13, 2018
Accepted, January 16, 2019